Smecticlike phase for modulated XY spins in two dimensions

M. Gabay

Laboratoire de Physique des Solides Laboratoire associé au CNRS, Université de Paris-Sud, Bâtiment 510,
91405 Orsay Cedex, France

M. Benakli

Department of Physics, Condensed Matter Section, ICTP, P.O. Box 586, 34014 Trieste, Italy

W. M. Saslow

Department of Physics, Texas A&M University, College Station, Texas 77843-4242

The row model for frustrated XY spins on a triangular lattice in two dimensions (2D) is used to study incommensurate (IC) spiral and commensurate (C) antiferromagnetic phases, in the regime where a C-IC transition occurs. Using fluctuating boundary conditions and specific histogram techniques, a detailed Monte Carlo (MC) study reveals more structure in the phase diagram than found in previous MC simulations of the full parameter space. On the C side, equilibrium configurations consist of alternating stripes of spiral phases of opposite chirality separated by walls of the C phase. For this same parameter regime, thermodynamic quantities are computed analytically using the NSCHA, a generalization of the self-consistent harmonic approximation appropriate for chiral systems. On the commensurate side of the C-IC boundary, NSCHA predicts an instability of the C phase. This suggests that the state is spatially inhomogeneous, consistent with the present MC result: it resembles the smectic-A phase of liquid crystals, and its existence implies that the Lifshitz point is at $T = 0$ for modulated XY spins in 2D. The connection between frustrated XY systems and the vortex state of strong type-II superconductors suggests that the smectic phase may correspond to a vortex liquid phase of superconducting layers. [S0163-1829(98)09217-0]

I. INTRODUCTION

Frustration is an ubiquitous phenomenon in condensed-matter physics. It occurs whenever several ground states of a system compete at different length scales. Examples of such a situation are noninteracting electrons in a tight-binding potential subjected to a uniform magnetic field,[1] networks of superconducting wires[2] or of Josephson junctions[3] in a field and spins with competing interactions.[4] In particular, frustrated magnetic systems have been used in the quantum case as realizations of the spin-liquid state[5] (advocated in the context of high-T_c superconductors). In the classical case, XY [$O(2)$] spins model the vortex state of layered, strong type-II superconductors.[6,7] Frustration manifests itself by the existence of chiral variables. The effect of this additional (Z_2) symmetry on phase transitions is still an open debate. For fully frustrated models there remains to establish whether the Z_2 and the $O(2)$ symmetries are broken at different temperatures or at the same temperature.[8–12] In the context of two-dimensional (2D) helimagnets this issue comes up when one studies the commensurate-incommensurate (C-IC) transition:[4] on the C side, the state is nonchiral whereas on the IC side chirality is coupled to the XY variables. Insight into this particular problem can be gained by studying the phase diagram of the row model, an anisotropic frustrated 2D XY model on a triangular lattice: it is a generalization of the fully frustrated XY model on the triangular lattice (FFTXY) where all the bonds strengths J are multiplied by η in the horizontal direction[13–15] (the FFTXY model corresponds to $\eta = 1$).

In order to study this system[16] and other IC structures,[17] a Monte Carlo (MC) algorithm with ''self-determined (fluctuating) boundary conditions'' (FBC) was developed. The resulting η versus T phase diagram indicated a continuous C-IC transition line starting at $\eta = 0.5$ for $T = 0$ and ending at a Lifshitz point[18] (LP) for $\eta_L \simeq 0.62$ and $T_L \simeq 0.42J$. Besides, increasing T at fixed η ($0.5 < \eta < \eta_L$) produced the following sequence of phases: an IC state at low T; then, across the C-IC transition, at $T_{\text{C-IC}}$, one moves into the C phase; lastly one reaches the paramagnetic (P) boundary at T_P. In this process one of the eigenvalues of the spin-wave stiffness matrix decreases uniformly as T varies from zero to $T_{\text{C-IC}}$, vanishes at $T_{\text{C-IC}}$, increases again in the C phase and becomes zero above T_P.

These MC results raise an issue, because they yield a thermodynamically stable commensurate state for $T \gtrsim T_{\text{C-IC}}$ and also because they predict a finite temperature LP: from the standpoint of critical phenomena, the C phase is in the same universality class as the ferromagnetic XY model; in the vicinity of the LP one may analytically compute the bare (unrenormalized) stiffness constant and one finds that it is very small. In this regime, the Kosterlitz-Thouless (KT) renormalization-group equations[19,20] show that vortex-antivortex pairs are unbound, implying that the C phase is thermodynamically unstable near the C-IC transition; so the renormalization group predicts a reentrant P phase and thus a zero-temperature Lifshitz point, at variance with the Monte Carlo results. Another indication that the LP may occur at $T = 0$ comes from the study of 2D modulated $O(N)$ spin systems exhibiting a C-IC transition; renormalization-group

analysis predicts[21] that the LP is at $T=0$ whenever $N>2$; numerical studies show that this also holds if $N=1$ (axial next-nearest-neighbor Ising model).[22] Interpolating to the case $N=2$ one might have then expected a zero-temperature LP for 2D XY systems: using a phase-only Hamiltonian, Garel and Doniach indeed reached this conclusion for the so-called J_1-J_2 model.[23]

The present paper reconciles these *a priori* conflicting results: In Sec. II, we present a MC algorithm allowing us to study incommensurate and spatially inhomogeneous states:[24] it combines FBC and specific boundary condition histograms designed for FBC. This approach allows us to analyze the data near the C-IC transition. Section III presents a MC study of the row model for $0.5<\eta<\eta_L$, for various T and η near the C-IC transition. Special attention is devoted to the C phase for $T\geq T_{C\text{-}IC}$. Our results suggest that the equilibrium structure is spatially inhomogeneous: Fig. 6 shows a striped structure, corresponding to the coexistence of domains of opposite chirality separated by walls of the collinear phase. Such a state resembles the smectic-A phase of liquid crystals. In this regime, we find that γ^{xx}—the spin rigidity in the horizontal (η-bond) direction—is zero, whereas γ^{yy}—the spin rigidity in the vertical direction—is strictly positive (Fig. 7). Stripes exist because the coupling between phase and chiral variables is relevant at all T when $\eta>0.5$. This coupling helps explain why domains of the chiral phase are present for $T\geq T_{C\text{-}IC}$. Moreover, fluctuations between a spatially homogeneous state (the incommensurate phase) and a spatially inhomogeneous spiral domain state (the striped phase) do not allow simple scaling analysis of critical quantities at $T_{C\text{-}IC}$ (Fig. 8).

These observations allow us to conclude that, in the phase diagram, the C and IC phases are separated by a smecticlike phase, and only come in contact at $T=0$ and $\eta=0.5$, so that the LP is indeed at $T=0$ for the 2D XY model. On the other hand, there is no re-entrant P phase between the C and IC regions.

Our numerical findings are further supported by analytic calculations, presented in Sec. IV. These use the new self-consistent harmonic approximation (NSCHA) method, a recently developed variational approach for frustrated systems.[10]

II. MONTE CARLO

A. Fluctuating boundary conditions

For incommensurate phases, the choice of periodic boundary conditions (PBC) in a MC simulation is not suitable, since these break the magnetic symmetry of the system. Instead, self-consistent boundary conditions, using FBC, have been proposed to overcome the problem.[16,25] The main feature of FBC is to add new dynamical variables Δ_α ($\alpha=1,2,\ldots,D$, where D is the dimensionality of the lattice) corresponding to a shift at the boundaries. In equilibrium the new ''boundary variables'' Δ_α will fluctuate around their *most probable value* Δ_α^0. For an $L\times L$ system of XY spins on a lattice, the FBC method amounts to imposing the following constraint on the phases $\theta(\vec{r})$ of the spins, at the boundary:

$$\theta(\vec{r}+nL\vec{u}_x+mL\vec{u}_y)=\theta(\vec{r})+nL\Delta_x+mL\Delta_y. \quad (1)$$

Using FBC allows us to preserve translational invariance: performing a change of variables

$$\theta(\vec{r})=\varphi(\vec{r})+\vec{\Delta}\cdot\vec{r}, \quad (2)$$

the constraint on φ becomes

$$\varphi(\vec{r}+nL\vec{u}_x+mL\vec{u}_y)=\varphi(\vec{r}). \quad (3)$$

In terms of the new variable φ the partition function of the $L\times L$ system with FBC is

$$Z_{\text{FBC}}=L^2\int_{-\pi/L}^{\pi/L}d^2\Delta\left(\int\cdots\int_{-\pi}^{\pi}\right.$$
$$\left.\times\prod_i d\varphi_i e^{-\beta[-(1/2)\Sigma_{i,j}J_{ij}\cos(\varphi_i-\varphi_j-\vec{\Delta}\cdot(\vec{r}_i-\vec{r}_j))]}\right).$$
$$(4)$$

Z_{FBC} can be factorized as a product of a set of partition functions, $Z(\vec{\Delta})$, each one corresponding to a fixed shift $\vec{\Delta}$ at the boundaries:

$$Z_{\text{FBC}}=L^2\int_{-\pi/L}^{\pi/L}Z(\vec{\Delta})d^2\Delta=L^2\int_{-\pi/L}^{\pi/L}d^2\Delta e^{-\beta L^2 f(\vec{\Delta})}, \quad (5)$$

where $f(\vec{\Delta})$ is the $2\pi/L$ periodic free-energy density associated with the shift $\vec{\Delta}$ at the boundary: $f(\vec{\Delta})=-T\ln(Z(\vec{\Delta}))/L^2$.

For a system with a helical phase at low temperature, $f(\vec{\Delta})$ displays a minimum for $\vec{\Delta}=\vec{\Delta}^0$ and for a spiral phase, the pitch $\vec{Q}_0$, is the $2\pi/L$ determination of $\vec{\Delta}_0$ such that $\varphi(\vec{r})\simeq0$ in equilibrium [see Eq. (2)]. Since the main contribution to the integral [Eq. (5)] comes from $\vec{\Delta}=\vec{\Delta}_0$, the components γ^{xx},γ^{yy} of the spin rigidity[20] are given by

$$\gamma^{xx}=\rho\left.\frac{\delta^2 f(\vec{\Delta})}{\delta\Delta_x^2}\right|_{\vec{\Delta}0}, \quad \gamma^{yy}=\rho\left.\frac{\delta^2 f(\vec{\Delta})}{\delta\Delta_y^2}\right|_{\vec{\Delta}0}, \quad (6)$$

where ρ is a (lattice-dependent) geometrical factor.

At low T and far from the C-IC boundary (where $\gamma^{xx}=0$), $\beta\gamma^{xx}\gg1$ and $\beta\gamma^{yy}\gg1$. Using Eqs. (5) and (6) then gives[16,24]

$$\gamma^{xx}=\frac{\rho}{L^2\chi_{\Delta_x}}, \quad \gamma^{yy}=\frac{\rho}{L^2\chi_{\Delta_y}}, \quad (7)$$

where $\chi_{\Delta_x}=\beta\langle(\Delta_x-\Delta_x^0)^2\rangle$ [respectively, $\chi_{\Delta_y}=\beta\langle(\Delta_y-\Delta_y^0)^2\rangle$] is the susceptibility for Δ_x (respectively, Δ_y).

B. Boundary condition histograms: Δ-histograms

In the previous section we showed that the partition function with FBC is a sum over partition functions $Z(\vec{\Delta})$. A practical way to perform this sum is to count the number of configurations obtained for each of the allowed values of Δ_x and Δ_y. Since Δ_x and Δ_y are defined modulo $2\pi/L$, this can be easily done by histograms in Δ_x and Δ_y, which we call Δ histograms.

Denoting by $P(\vec{\Delta}) \equiv P(\Delta_x, \Delta_y)$ the probability distribution for $\vec{\Delta}$, the Δ-histogram free-energy density is obtained from

$$f(\vec{\Delta}) = -\frac{1}{\beta L^2} \ln(P(\vec{\Delta})) + \text{const.} \qquad (8)$$

If $f(\vec{\Delta})$ has a deep minimum for $\vec{\Delta} = \vec{\Delta}^0$, the zeroes of the first derivative of the free energy yield the value of $\vec{\Delta}^0$. The second derivatives of the free energy computed for $\vec{\Delta} = \vec{\Delta}^0$ give the components of the spin-wave stiffness γ, by Eq. (6). But even if $P(\vec{\Delta})$ is not sharply peaked (see below), the histograms allow us to compute any thermodynamic observable as an average over $P(\vec{\Delta})$.

This algorithm is especially useful when (i) one approaches a critical C-IC transition: $\vec{\Delta}$ undergoes large fluctuations and Eq. (7) breaks down; histograms give much more accurate results and are well suited to scaling analysis, (ii) equilibrium configurations correspond to inhomogeneous structures: in that case, histograms yield multipeak structures. For instance, if domains of the C and IC phases coexist near $T_{\text{C-IC}}$ the free energy will display minima at $\vec{\Delta} = \vec{0}$ and at $\pm \vec{\Delta}^0$.

III. NUMERICAL ANALYSIS OF THE ROW MODEL NEAR THE C-IC TRANSITION

Since the incommensurability is only present in the x (η bonds) direction we used hybrid boundary conditions: PBC in the y direction and FBC in the x direction. A standard Metropolis algorithm was applied to the spin angles and to the boundary shift in the x direction. Lattices sizes ranged from 18^2 to 48^2 and the number of MCS/spin was of order $10^5 - 10^6$. Typically the first 10^4 steps were discarded for equilibration. In contrast to our previous study of this system,[16] Δ histograms were included here. These were used to determine Q_0 (the x component of the wave vector) as well as the spin-wave stiffnesses along x and y. In addition, we monitored (i) the staggered chiralities $\Sigma = \langle \sigma \rangle$ with

$$\sigma = \frac{1}{N_P} \sum_{\{P\}} \frac{\Sigma_{\langle kl \rangle \in P} \sigma_{kl}}{\Sigma_{\langle kl \rangle \in P} \sigma_{kl}(T=0)}, \qquad (9)$$

where P refers to plaquettes in the same chiral state at $T = 0$ and

$$\sigma_{kl} = \frac{1}{2\pi}(\theta_k - \theta_l) \qquad (10)$$

[for Eq. (10), the angular determination of the term in parenthesis is taken in the interval $[-\pi, +\pi]$ (see Ref. 10)]. (ii) The chiral susceptibility

$$\chi_\sigma = \frac{1}{T} \langle \sigma^2 - \Sigma^2 \rangle, \qquad (11)$$

(iii) The Binder order parameter for chiralities

$$g_\sigma = \frac{1}{2} \left[3 - \left(\frac{\langle \sigma^4 \rangle}{\langle \sigma^2 \rangle} \right) \right]. \qquad (12)$$
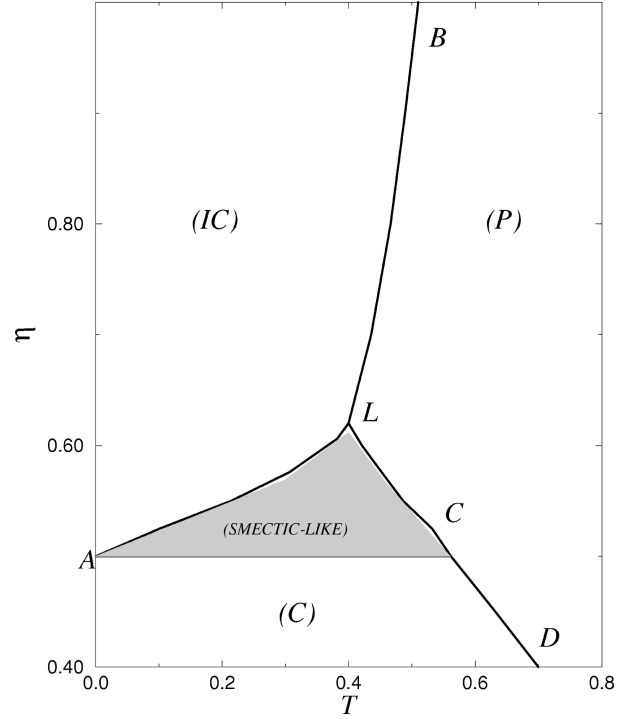

FIG. 1. MC phase diagram for the row model, in the (η, T) plane.

A. Study of the C-IC line at fixed η

In the phase diagram of Fig. 1, AL is a line separating the spiral incommensurate phase from the commensurate layered antiferromagnetic C phase. It is characterized by a divergence of the chiral susceptibility and by the *continuous vanishing* of the x component of the spin stiffness (Fig. 2). The y component of the spin stiffness, on the other hand, does not show any nonanalyticity near AL. In this part, we keep the value η fixed and we vary the temperature. Typically we chose $\eta = 0.575$ and $\eta = 0.55$. Starting from the low-temperature phase, we observe that $\gamma^{xx} \to 0$ and that simul-
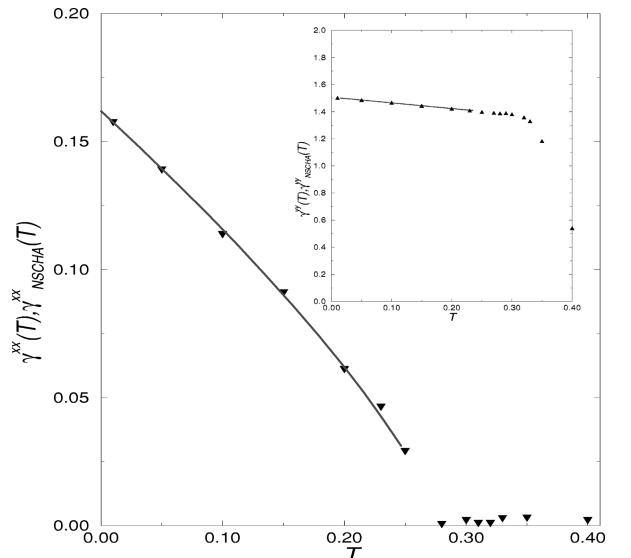

FIG. 2. Monte Carlo stiffnesses in the x and y (inset) directions versus T for the row model when $\eta = 0.575$. Triangles represent MC data, solid lines are the NSCHA predictions.
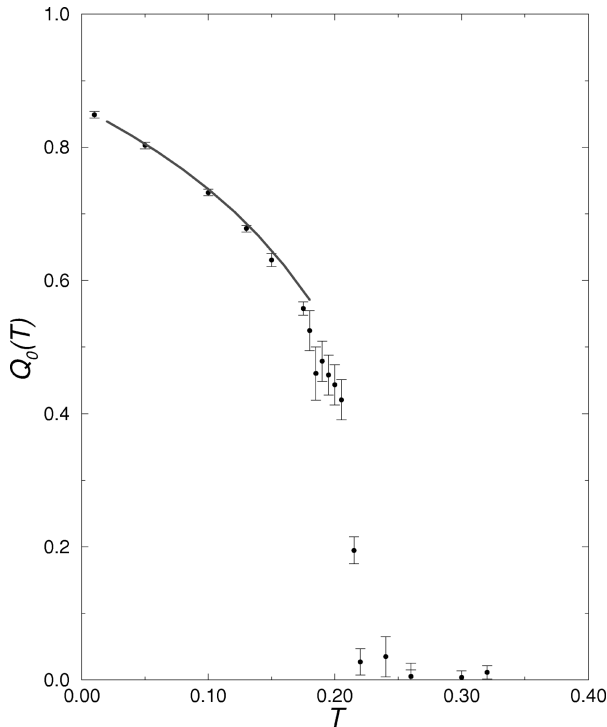
FIG. 3. $Q_0(T)$ versus T for $\eta = 0.55$. Filled circles represent MC data and the solid line is the NSCHA prediction.

FIG. 4. $P(Q_x)$ versus Q_x for $\eta = 0.55$ and $T = 0.19J$.

taneously the chiral susceptibility diverges as one approaches AL, Fig. 2. This behavior can be understood as follows: The Coulomb-gas analysis by Eikmans et al. of the generalized Villain model,[26] when generalized to the row model, gives[27]

$$\gamma^{xx} \propto \frac{1}{\chi_\sigma}. \tag{13}$$

Chiral variables and spin-angle variables are coupled in the IC phase; thus γ^{xx} can go to zero in a continuous fashion, rather than jump, on crossing AL. Similarly from the same Coulomb-gas analysis, one expects that γ^{yy} is well behaved across AL (Fig. 2). Figure 3 shows that Q_0 also goes to zero (mod 2π) at $T_{\text{C-IC}}$. At first sight, the system appears to simply evolve from a homogeneous IC phase into a homogeneous C phase as $T \to T_{\text{C-IC}}$ from below. If this picture were correct, here is what histograms would yield: at low T, $P(\vec{\Delta})$ would display two maxima at $\pm \vec{\Delta}^0$ (corresponding to the two possible handedness of the spiral in the IC state). As $T \to T_{\text{C-IC}}$, the two peaks would merge into a single peak, and, for $T > T_{\text{C-IC}}$, $P(\vec{\Delta})$ would be a Gaussian, centered at $\Delta_x = 0$. By Eqs. (6) and (8), we would expect $\gamma^{xx} > 0$ for $T > T_{\text{C-IC}}$.

By contrast, here is what our simulation yields: at low T we do get the two maxima at $\pm \vec{\Delta}^0$ and as $T \to T_{\text{C-IC}}$ they move closer to each other. However, they do not merge: the peaks at $\pm \vec{\Delta}^0$ remain sharp and in addition a third peak develops at $\Delta_x = 0$, such that Δ histograms show a three-peak structure for $T > T_{\text{C-IC}}$. There is a central peak at $\Delta_x = 0$ and two side peaks centered at T dependent, finite values $\pm \Delta_0$. For sizes 48^2 and for simulations using large enough MCS/spin the relative weight of the lateral peaks compared to the central peak is roughly one. Furthermore, this structure
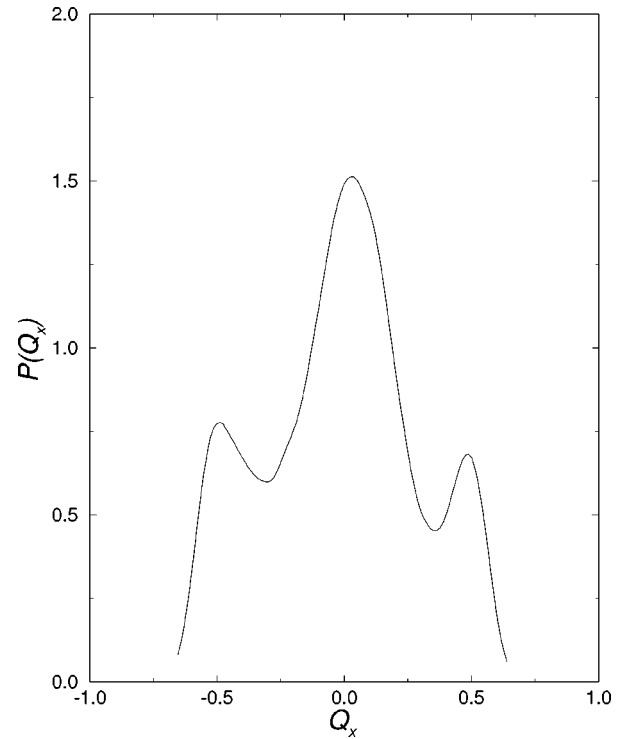
of the Δ histogram is observed in a wide range of temperatures above $T_{\text{C-IC}}$. For instance we show the histogram for $T \gtrsim T_{\text{C-IC}}$ (Fig. 4). The structure of $P(\vec{\Delta})$ could have two origins: it could be associated with a first-order transition, and the fact that the multipeak structure survives for $T > T_{\text{C-IC}}$ could be linked to hysteresis effects, or it could be due to the occurrence of a nonhomogeneous thermodynamic phase.

The first-order scenario is at variance with the observed temperature dependence of γ_{xx} in two respects: (i) For $T \to T_{\text{C-IC}}$ from below, both γ_{xx} and χ_σ^{-1} go continuously to zero, as indicated by Eq. (13). (ii) For $T > T_{\text{C-IC}}$ up to the paramagnetic boundary, we find that $\gamma_{xx} = 0$ (see Fig. 2); if we tried to explain this property in the framework of a first-order transition, this would mean that the system is in a spinodal state over a wide range of temperature, which is rather unlikely.

Instead, we suggest that these data can be consistently interpreted if one considers the possibility of a thermodynamically inhomogeneous phase for $T > T_{\text{C-IC}}$. We mentioned in the introduction that systems with competing interactions may lead to inhomogeneous ground states consisting of ordered domains separated by domain walls.[28–32] Our simulations reveal that the commensurate phase of the row model may well be such an example of stripe phases.

From the shape of $P(Q_x)$ we see that a measure of (the equilibrium value of) Q_x at any point of the lattice gives 0 with probability $\frac{1}{2}$, $+Q_0$ with probability $\frac{1}{4}$ and $-Q_0$ with probability $\frac{1}{4}$ [$+Q_0$ and $-Q_0$ are the secondary maxima of $P(Q_x)$, see Fig. 4]. The connection between the equilibrium value of Q_x and the plaquette chirality [Eq. (10)] implies that the chirality of any site of a given sublattice will be positive, negative, and zero with probability $\frac{1}{4}$, $\frac{1}{4}$, and $\frac{1}{2}$, respectively: indeed, if we had a homogeneous phase characterized by
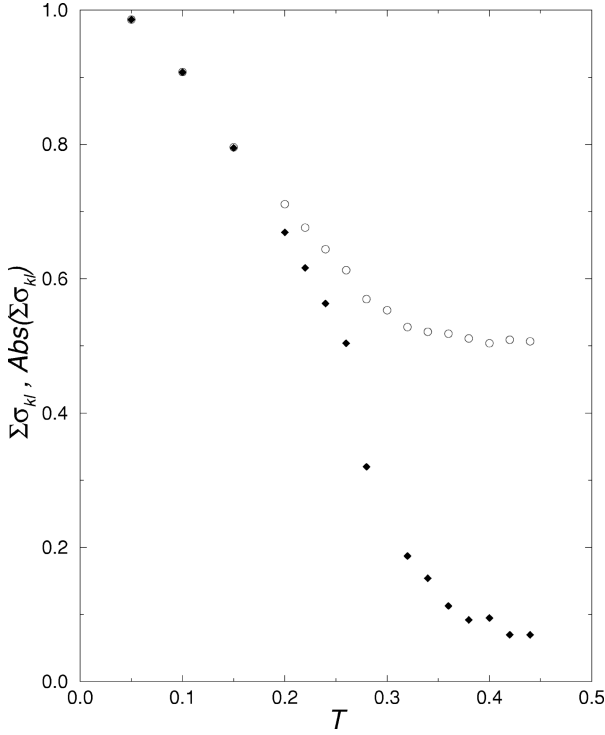
FIG. 5. MC determination of the plaquette chirality $\Sigma_{\langle kl\rangle \in P}\sigma_{kl}$ (filled diamonds) and of the absolute value of the plaquette chirality $Abs(\Sigma_{\langle kl\rangle \in P}\sigma_{kl})$ (open circles) versus T for $\eta=0.575$.
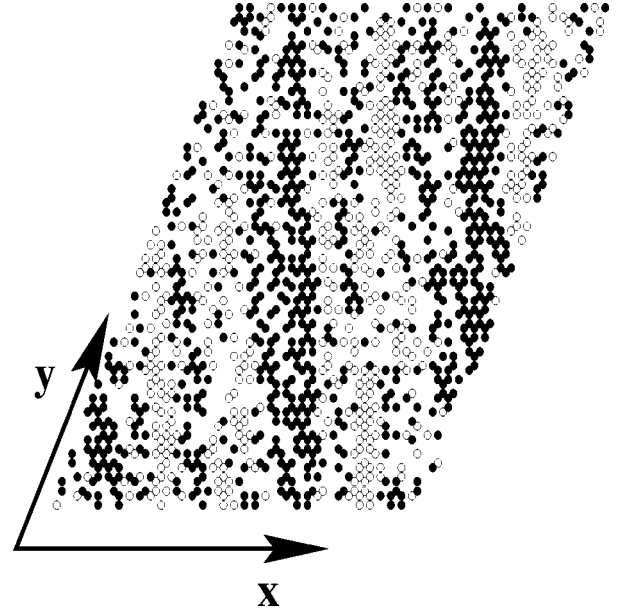

FIG. 6. Snapshot of chiralities on each plaquette of a 36^2 triangular lattice. $\eta=0.575$ and $T=0.4J$. Filled circles represent plaquettes with the correct sign, i.e., in the same chiral state as at $T=0$. Open circles correspond to plaquettes with the wrong sign, that is such that the chirality has changed compared to $T=0$. Plaquettes with zero chirality (no symbol) are obtained in-between the two. One clearly sees a stripe structure of filled circles and open circles separated by domain walls of zero chirality.

$Q_x=+Q_0$ over the entire system, the chiralities of the plaquettes of a given sublattice—denoted by A—would all have the same sign, say positive; similarly, if we had $Q_x=-Q_0$ over the entire system, the chirality of A would be negative for all the plaquettes; lastly, if $Q_x=0$ over the entire system, the chirality of A would be zero for all the plaquettes. Since the values of Q_x are distributed according to $P(Q_x)$, we deduce the above-mentioned distribution for the chiralities of any site of A.

Figure 5 precisely confirms this analysis. It is a plot (as a function of T) of the staggered chirality [Eq. (10)] and of the absolute value of the chiralities [where we replace $\Sigma_{\langle kl\rangle \in P}\sigma_{kl}$ by $Abs(\Sigma_{\langle kl\rangle \in P}\sigma_{kl})$ in Eq. (9)], for $\eta=0.575$. These two quantities give access to the number of plaquettes with positive, negative, and zero chirality one each sublattice (see Ref. 10). We see that, for $T=0.4J$, well above the C-IC transition temperature, in what should be the commensurate phase, i.e., a state with zero chirality, 25% of the plaquettes have a positive chirality, 25% of the plaquettes have a negative chirality, and 50% of the plaquettes have no chirality. With these weights, averaging Q_x over the system yields $Q_x=0$.

The shape of $P(Q_x)$ also signals the breakdown of the fluctuation-dissipation theorem. The correct procedure required to extract the value of γ^{xx} is to average $\delta^2 f(\vec\Delta)/\delta\Delta_x^2$ over the distribution $P(\vec\Delta)$. If the dominant contribution to $P(\vec\Delta)$ comes from a single value, $\vec\Delta=\vec\Delta_0$, this yields Eq. (6), which gives the most probable value of γ^{xx}. If $P(\vec\Delta)$ has a multipeak structure, as is the case here, Eq. (6) is not valid: choosing for $\vec\Delta_0$ the value of $\vec\Delta$ corresponding to $Q_x=+Q_0$, or to $Q_x=-Q_0$, or to $Q_x=0$ which is the mean value of

$P(\vec\Delta)$, would give different values for γ^{xx} but such that $\gamma^{xx}>0$. By contrast, the average of $\delta^2 f(\vec\Delta)/\delta\Delta_x^2$ over $P(\vec\Delta)$ leads to $\gamma_{xx}=0$ (see Fig. 2). So averages and most probable values do not coincide.

The picture that emerges from the previous results is that of an inhomogeneous structure for $T>T_{\text{C-IC}}$: domains of the spiral phase with pitch $+Q_0$ coexist with domains of the spiral phase with pitch $-Q_0$, and the two types are separated by domain walls of the collinear phase. It is known that the transition from a homogeneous phase (the IC state) to a domain structure can be continuous,[33] which is consistent with our results. The spatial configuration of the domains is visualized in Fig. 6, which is a snapshot of the chiralities for $\eta=0.575$ and $T=0.4J$. The morphology of the state is that of a striped phase. Note that the normal to the direction of the stripes correlates with x (the direction of the η bonds). We dub this structure a smecticlike phase: it is solidlike along y ($\gamma^{yy}>0$) but has no rigidity along x ($\gamma^{xx}=0$); its effective free energy in the hydrodynamic limit is similar to that of a smectic system (Ref. 34).

B. Study of the C-IC line at fixed T

To map out the domain of stability of the striped phase in the (η,T) plane, we keep T fixed and we vary η. Figure 7 shows γ_{xx} versus η for $T=0.2J$ and $T=0.4J$; in the region delimited by lines AC ($\eta=0.5$) and AL we get $\gamma_{xx}=0$ and one expects a striped phase there. In other words AL separates an incommensurate phase from an inhomogeneous, noncollinear state.

We have also sought for an analytical evidence of the inhomogeneous state in region ALC of the phase diagram
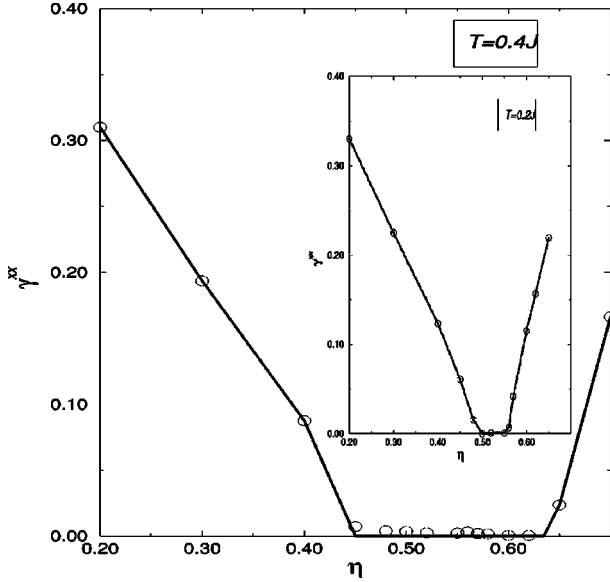
FIG. 7. MC data for γ^{xx}, versus η. The lattice size is 48^2. γ^{xx} is obtained from the histogram in Δ modulo $2\pi/L$. The region where $\gamma^{xx}=0$ corresponds to the domain of stability of the stripe phase. T is fixed: $T=0.4J$ (inset $T=0.2J$).

Fig. 1. The next section presents results using NSCHA, a variational technique appropriate for frustrated systems: if one seeks a uniform collinear solution in region ALC, one finds that $\gamma^{xx}<0$; this behavior stems from the fact that the system is thermodynamically unstable with respect to the formation of domains having either $Q_x=+Q_0$ or $Q_x=-Q_0$, the two types connecting via domain walls of the collinear ($Q_x=0$) phase. The breakdown of linear response and the properties of γ^{xx} are hallmarks of the physics of dipolar magnets and of spin glasses.[28–30]

IV. NSCHA FOR THE COMMENSURATE AND INCOMMENSURATE REGIMES

In a previous paper we introduced the new self-consistent harmonic approximation (NSCHA),[10] a variational technique appropriate for frustrated systems. The main feature of this approach is that it preserves the coupling between the chiral ground states of the system, and that it takes long-wavelength chiral fluctuations into account. Chiral and phase (spin-angle) variables remain coupled at all temperatures T. We now apply this method to the row model.

A. The NSCHA variational method

The Hamiltonian for XY spins characterized by spin angles $\{\theta_i\}$, reads

$$H=-\sum_{\langle ij\rangle} J_{ij}\cos(\theta_i-\theta_j), \qquad (14)$$

where the J_{ij} are nearest-neighbor interactions. For frustrated systems the sign of the product of the J_{ij} over the links of a plaquette P is negative and this may lead to noncollinear configurations in thermal equilibrium. The variational method seeks to approximate H [Eq. (14)] by a harmonic Hamiltonian H_0. We rewrite the θ_i in Eq. (14) as

$$\theta_i=\theta_i^0+\varphi_i \qquad (15)$$

with $\theta_i^0=\langle\theta_i\rangle_{H_0}$ and

$$H_0=\frac{1}{2}\sum_{\langle ij\rangle} \widetilde{J}_{ij}(\varphi_i-\varphi_j)^2. \qquad (16)$$

Hamiltonian Eq. (14) is then mapped onto the NSCHA effective Hamiltonian H_{NSCHA},[10]

$$H_{\text{NSCHA}}=-\sum_{\langle ij\rangle} J_{ij}\cos(\theta_i^0-\theta_j^0)\cos(\varphi_i-\varphi_j)$$

$$-\frac{1}{2T}\sum_{\langle ij\rangle}\sum_{\langle kl\rangle} J_{ij}J_{kl}\sin(\theta_i^0-\theta_j^0)\sin(\theta_k^0-\theta_l^0)$$

$$\times\sin(\varphi_i-\varphi_j)\sin(\varphi_k-\varphi_l). \qquad (17)$$

We then average Eq. (17) over H_0 [Eq. (16)] and minimize with respect to the variational parameters[10] θ_i^0 and $\widetilde{J}_{ij}$ to obtain the NSCHA variational equations.

In this ensemble we can compute the spin-wave stiffness matrix. Its eigenvalues are $\gamma_{\text{NSCHA}}^{xx}$ and $\gamma_{\text{NSCHA}}^{yy}$:

$$\gamma_{\text{NSCHA}}^{xx}=\frac{1}{N}\sum_{\langle ij\rangle} J_{ij}\cos(\theta_i^0-\theta_j^0)(\vec{u}_{ij}\cdot\vec{u}_x)^2 e^{-y_{ij}/2}$$

$$-\frac{1}{N}\frac{1}{T}\sum_{\langle ij\rangle}\sum_{\langle kl\rangle} J_{ij}J_{kl}(\vec{u}_{ij}\cdot\vec{u}_x)(\vec{u}_{kl}\cdot\vec{u}_x)$$

$$\times e^{-(y_{ij}+y_{kl}+y_{ik}+y_{jl}-y_{il}-y_{jk})/2}$$

$$\times[\cos(\theta_i^0-\theta_j^0)\cos(\theta_k^0-\theta_l^0)$$

$$+\sin(\theta_i^0-\theta_j^0)\sin(\theta_k^0-\theta_l^0)], \qquad (18)$$

where $\vec{u}_x$ is the unit vector in the horizontal direction, $\vec{u}_{ij}$ is the vector connecting nearest-neighbor sites i and j, and $y_{ij}=\langle(\varphi_i-\varphi_j)^2\rangle_{H_0}$. For $\gamma_{\text{NSCHA}}^{yy}$ we replace $\vec{u}_x$ by $\vec{u}_y$ the unit vector in the vertical direction.

B. NSCHA for the row model

Applying NSCHA to the row model gives two types of solutions.

(a) Commensurate solutions: They are characterized by

$$\theta_i^0-\theta_j^0=\vec{Q}^0\cdot\vec{u}_{ij} \quad (\text{mod}2\pi) \qquad (19)$$

with

$$Q_x^0=0; \quad Q_y^0=\frac{2\pi}{\sqrt{3}} \quad (\text{mod}2\pi) \qquad (20)$$

and by nearest-neighbor couplings $\widetilde{J}_{ij}$. There are only two independent interactions namely $\widetilde{J}_{ij}=\widetilde{\eta}\widetilde{J}$ for i and j along the horizontal direction, and $\widetilde{J}_{ij}=\widetilde{J}$ otherwise. These satisfy the following equations:

$$\widetilde{J}=Je^{-(T/\pi\widetilde{J})\tan^{-1}[(1+2\widetilde{\eta})^{-1/2}]}, \qquad (21)$$

$$\widetilde{\eta}\widetilde{J}=-\eta Je^{-(T/\pi\widetilde{\eta}\widetilde{J})\tan^{-1}[\widetilde{\eta}(1+2\widetilde{\eta})^{-1/2}]}. \qquad (22)$$

Equations (21) and (22) can be self-consistently satisfied without restriction for $\eta \leq 1/2$. However, if $\eta > 1/2$ Eqs. (21) and (22) have no solution when $T \leq (J/\eta)\ln(2\eta)$; this was to be expected, since the stable state of the system is a spiral structure at low T, for $\eta > 1/2$.

(b) Incommensurate solutions: They correspond to

$$\theta_i^0 - \theta_j^0 = \vec{Q}^0 \cdot \vec{u}_{ij} \quad (\mathrm{mod}\, 2\pi) \qquad (23)$$

with

$$Q_x^0 = Q_0(T); \quad Q_y^0 = \frac{2\pi}{\sqrt{3}} \quad (\mathrm{mod}\, 2\pi). \qquad (24)$$

The variational equations can only be solved numerically. Just as for the FFT*XY* model, the $\tilde{J}_{ij}$ are no longer short-range interactions (for large R, $\tilde{J}_{ij} \sim 1/|\vec{r}_i - \vec{r}_j|^6$ see Ref. 10) and the sign of $\tilde{J}_{ij}$ varies with the relative orientation of i and j. Knowledge of the $\tilde{J}_{ij}$ allows us[10] to compute the free energy, $Q_0(T)$, $\gamma_{\mathrm{NSCHA}}^{xx}$, $\gamma_{\mathrm{NSCHA}}^{yy}$ [Eq. (18)], and the staggered chirality σ_{NSCHA} as a function of T *for all* η.

For *all* $\eta < 0.5$ the lowest free energy is obtained for the commensurate solution and up to the C-P boundary (line *CD* in Fig. 1) $\gamma_{\mathrm{NSCHA}}^{xx} > 0$.

For $0.5 < \eta < \eta_L$, the IC solution has the lowest energy at low T ($T < T_{\text{C-IC}}$). As seen in Figs. 2 and 3, NSCHA and MC results agree closely except in the vicinity of $T_{\text{C-IC}}$, where defects are expected to play an important role (see our previous paper, Ref. 10). In that regime $\gamma_{\mathrm{NSCHA}}^{xx} > 0$. For $T > T_{\text{C-IC}}$ the variational equations favor a commensurate configuration, but we find that $\gamma_{\mathrm{NSCHA}}^{xx} < 0$: the solution is thermodynamically unstable. By this we mean that NSCHA yields a C solution in the region *ALC* of the phase diagram, but that fluctuations around the solution (given by $\gamma_{\mathrm{NSCHA}}^{xx}$) generate an instability.

We summarize our results as follows.

(1) In the η, T plane, the transition between the spiral phase and the C phase is only seen at point A (that is, at zero temperature). Consequently, the Lifshitz point is at $T = 0$ for the 2D *XY* model.

(2) The existence of the striped phase suggests that chiral variables and phase variables remain strongly coupled at all T. This may explain why, despite the fact that $\gamma_{xx} = 0$ in the striped phase, vortices do not unbind (leading to a reentrant paramagnetic phase). The relevance of this coupling had already been emphasized in our study of the fully frustrated case ($\eta = 1$).

(3) The existence of the inhomogeneous state affects scaling analyses near the IC-stripe phase boundary (line *AL*): Fig. 8 shows the Binder order parameter Eq. (12) as a function of T for $\eta = 0.575$. We do not observe a clear intersection at the critical temperature. A similar feature had been pointed out by Olsson in his study of fully frustrated *XY* spins on a 2D square lattice (Ref. 12).

(4) Because the striped phase is spatially inhomogeneous, it is not easy to define appropriate boundary conditions for the MC simulation. Uniform twists will produce frustration.

The present work has revealed the existence of a smecticlike phase. This raises the question of the nature of the transition between the striped phase and the P phase (line
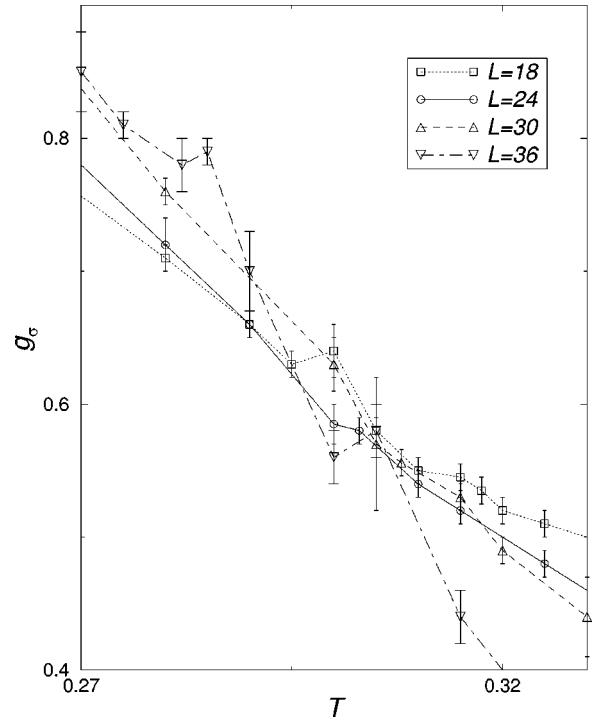

FIG. 8. Binder order parameter g_σ versus T for various sizes [Eq. (12)].

LC) and also between the striped phase and the commensurate phase (line *AC*); for instance, if the transition line *LC* is not KT like, one also needs to understand the nature of the critical regime along *CD*: for $\eta \leq 0.5$ one recovers a KT transition so there has to be some crossover. Work is in progress to clarify that issue.

V. CONCLUSION

Using detailed Monte Carlo simulations we have studied the commensurate-incommensurate transition of the two dimensional *XY* model on a triangular lattice. Our study shows that this transition only occurs at $T = 0$. At finite temperature, the incommensurate structure evolves into a striped phase made up of domains of left- and right-handed spirals separated by walls. The domain walls consist of the collinear structure. This state resembles the smectic-A phase of liquid crystals. The nature of the phase transitions between the striped phase and the ordered phases or between the striped phase and the paramagnetic phase is an open problem. Analytical calculations using NSCHA (a variational approach well suited for noncollinear structures) support the MC results. The connection between frustrated *XY* models and the vortex state of layered type-II superconductors suggest to view the smectic phase as a vortex liquid state. This regime would appear to be an intermediate phase between the superconducting and the metallic states, critical in one subspace and quasiordered in the other.

[1] D. R. Hofstadter, Phys. Rev. B **14**, 2239 (1976).

[2] Y. Hasegawa, M. Kohmoto, and G. Montambaux, Phys. Rev. B **48**, 1119 (1993).

[3] I.-J. Hwang and D. Stroud, Phys. Rev. B **54**, 14 978 (1996).

[4] H. T. Diep, *Magnetic Systems with Competing Interactions* (World Scientific, Singapore, 1994).

[5] V. Kalmeyer and R. B. Laughlin, Phys. Rev. B **39**, 11 879 (1989).

[6] Y-H. Li and S. Teitel, Phys. Rev. B **47**, 359 (1993); T. Chen and S. Teitel, Phys. Rev. Lett. **72**, 2085 (1994); M. Franz and S. Teitel, *ibid.* **73**, 480 (1994); T. Chen and S. Teitel, *ibid.* **74**, 2792 (1995).

[7] G. Blatter *et al.*, Rev. Mod. Phys. **66**, 1125 (1994).

[8] There is a vast literature on this problem; see for instance references quoted in Refs. 9–12.

[9] M. Benakli and E. Granato, Phys. Rev. B **55**, 8361 (1997).

[10] M. Benakli, H. Zheng, and M. Gabay, Phys. Rev. B **55**, 278 (1997).

[11] J. V. José and G. Ramirez-Santiago, Phys. Rev. Lett. **77**, 4849 (1996).

[12] P. Olsson, Phys. Rev. Lett. **75**, 2758 (1995).

[13] G. Parker, W. M. Saslow, and M. Gabay, Phys. Rev. B **43**, 11 285 (1991).

[14] W.-M. Zhang, W. M. Saslow, M. Gabay, and M. Benakli, Phys. Rev. B **48**, 10 204 (1993).

[15] H. Kawamura, Prog. Theor. Phys. Suppl. **101**, 545 (1990).

[16] W. M. Saslow, M. Gabay, and W.-M. Zhang, Phys. Rev. Lett. **68**, 3627 (1992).

[17] M. Collins and W. M. Saslow, Phys. Rev. B **53**, 8533 (1996).

[18] R. M. Hornreich, M. Luban, and S. Strikman, Phys. Rev. Lett. **35**, 1678 (1975).

[19] J. M. Kosterlitz and D. J. Thouless, J. Phys. C **6**, 1181 (1973); J. V. José, L. P. Kadanoff, S. Kirkpatrick, and D. R. Nelson, Phys. Rev. B **16**, 1217 (1977).

[20] P. Minnhagen, Rev. Mod. Phys. **59**, 1001 (1987).

[21] P. Azaria, B. Delamotte, F. Delduc, and T. Jolicoeur, Nucl. Phys. **B408**, 485 (1993).

[22] W. Selke, in *Phase Transitions and Critical Phenomena*, edited by C. Domb and J. L. Lebowitz (Academic, New York, 1992), Vol. 15, p. 2.

[23] T. A. Kaplan, Phys. Rev. Lett. **44**, 760 (1980); T. Garel and S. Doniach, J. Phys. C **13**, L887 (1980).

[24] M. Benakli, M. Gabay, and W. M. Saslow, Eur. Phys. J. B **1**, 197 (1998).

[25] P. Olsson, Phys. Rev. Lett. **73**, 3339 (1994).

[26] H. Eikmans, J. E. van Himbergen, H. J. F. Knops, and J. M. Thjissen, Phys. Rev. B **39**, 11 759 (1989).

[27] Equation (13) can be understood with the help of the following argument: using definition (10), the staggered chirality order parameter Σ [Eq. (9)] is expressed as a sum over nearest-neighbor phase differences in the x direction. This sum is proportional to Q_x, so that χ_σ [Eq. (11)] contains the fluctuations of Q_x described by χ_{Q_x}. By Eq. (7) one gets Eq. (13).

[28] M. Gabay and T. Garel, J. Phys. (Paris) **46**, 5 (1985); Phys. Rev. B **33**, 6281 (1986).

[29] A. Kashuba, Ar. Abanov, and V. L. Povrosky, Phys. Rev. Lett. **77**, 2554 (1996).

[30] K. H. Fischer and J. A. Hertz, in *Spin Glasses* (Cambridge University Press, Cambridge, 1991).

[31] G. Uimin and A. Pimpinelli, Phys. Rev. E **49**, 1123 (1994).

[32] A. Pimpinelli, G. Uimin, and J. Villain, J. Phys.: Condens. Matter **3**, 4693 (1991); J. L. Cardy, M. P. M. den Nijs, and M. Schick, Phys. Rev. B **27**, 4251 (1983).

[33] M. den Nijs, in *Phase Transitions and Critical Phenomena*, edited by C. Domb and J. L. Lebowitz (Academic, New York, 1988), Vol. 12, p. 219.

[34] A. R. Day, T. C. Lubensky, and A. J. McKane, Phys. Rev. A **27**, 1461 (1983); see also, D. R. Nelson, in *Phase Transitions and Critical Phenomena*, edited by C. Domb and J. L. Lebowitz (Academic, New York, 1983), Vol. 7, p. 89.